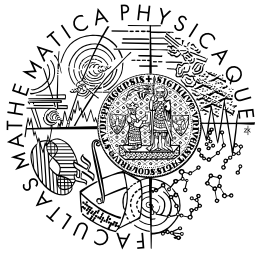

FACULTY
OF MATHEMATICS
AND PHYSICS
Charles University

SUMMARY OF DOCTORAL THESIS

Vojtěch Patočka

Maxwell-type viscoelasticity in small and large deformations of planetary mantles

Department of Geophysics

Supervisor of the doctoral thesis: prof. RNDr. Ondřej Čadek, CSc.
Study programme: Physics
Study branch: Geophysics

Prague 2018

Title: Maxwell-type viscoelasticity in small and large deformations of planetary mantles

Author: Mgr. RNDr. Vojtěch Patočka

Department: Department of Geophysics

Supervisor: prof. RNDr. Ondřej Čadek, CSc., Department of Geophysics

Abstract: A present limitation of global-scale simulations of planetary interiors is that they assume a purely viscous or viscoplastic flow law for solid rock, i.e. elasticity is ignored. This is not a good assumption in the cold and strong outermost mantle layer known as the lithosphere, which seems to maintain its elastic properties even on time scales corresponding to the geological processes of subduction or sedimentation. Here we overcome such simplification and present a numerical tool for modelling visco-elasto-plastic mantle convection. The most promising new feature of the resulting models is related to the ability of viscoelastic materials to remember deformation experienced in the past. Thus, the growing viscoelastic lithosphere of a cooling planet, when subject to internal or surface loading, can store information about its thickness at the time of loading. This phenomena is consistent with datasets of the effective elastic thicknesses determined in flexure studies and we label it here as the "stress memory effect". Attention is also paid to the theoretical foundations of viscoelasticity. We review the approaches that are commonly used to formulate Maxwell-type constitutive equations and thoroughly analyze the condition of material objectivity in a search for objective stress rate that fits Maxwell's original idea the best. While the main focus of the thesis lies in the field of large deformations, small deformations of planetary mantles are addressed too. We solve the traditional problem of glacial isostatic adjustment on a rotating Earth and analyze the accompanying changes in the rotational, gravitational and elastic energy of the planet.

Keywords: Viscoelasticity, Maxwell fluid, Numerical modelling

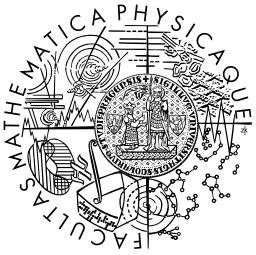

MATEMATICKO-FYZIKÁLNÍ FAKULTA
Univerzita Karlova

Autoreferát dizertační práce

Vojtěch Patočka

Viskoelasticita Maxwellova typu v malých i velkých deformacích plášťů terrestrických planet

Katedra geofyziky

Školitel:	prof. RNDr. Ondřej Čadek, CSc.
Studijní program:	Fyzika
Studijní obor:	Geofyzika

Praha 2018

Dizertace byla vypracována na základě výsledků získaných v letech 2013-2018 během doktorandského studia na Katedře geofyziky MFF UK a na oddělení Earth Sciences ETH Zurich.

Dizertant:
Mgr. RNDr. Vojtěch Patočka
Katedra geofyziky MFF UK
V Holešovičkách 2, 180 00 Praha 8

Školitel:
prof. RNDr. Ondřej Čadek, CSc.
Katedra geofyziky MFF UK
V Holešovičkách 2, 180 00 Praha 8

Oponenti:
Dr. Nicola Tosi
Zentrum für Astronomie und Astrophysik
Technische Universität Berlin
Skr. EW
8-1, Hardenbersgstrasse 36
D-10623 Berlin
Germany

Mgr. Vít Průša, Ph.D.
Matematický ústav UK
Sokolovská 83
Praha 8

Předsedkyně oborové rady:
Doc. RNDr. Hana Čížková, PhD.
Katedra geofyziky MFF UK
V Holešovičkách 2, 180 00 Praha 8

Obhajoba dizertace se koná dne 29.6.2018 v 10:00 hodin před komisí pro obhajoby dizertačních prací v oboru Geofyzika v budově MFF UK, Ke Karlovu 3, Praha 2, v místnosti M252.

S dizertací je možno se seznámit v PGS MFF UK, Ke Karlovu 3, Praha 2.

Název: Viskoelasticita Maxwellova typu v malých i velkých deformacích plášťů terrestrických planet

Autor: Mgr. RNDr. Vojtěch Patočka

Katedra: Katedra geofyziky

Vedoucí disertační práce: prof. RNDr. Ondřej Čadek, CSc., Katedra geofyziky

Klíčová slova: Viskoelasticita, Maxwellova tekutina, Numerické modelování

Abstrakt: Současná limitace globálních simulací plášťů terrestrických planet spočívá v tom, že uvažují čistě viskózní nebo visko-plastické tečení plášťových hornin, a tedy zanedbávají jejich elasticitu. Tato aproximace není vyhovující ve studené a pevné svrchní vrstvě pláště, známé jako litosféra, která si uchovává elastické vlastnosti i na časových škálách odpovídajících geologickým procesům subdukce a sedimentace. V této práci překonáváme toto zjednodušení a představujeme numerický nástroj pro modelování visko-elasto-plastické plášťové konvekce. Zajímavá vlastnost našich simulací pramení ze schopnosti viskoelastického materiálu pamatovat si prodělanou deformaci. A tak postupně mohutnějící litosféra chladnoucí planety, vystavená vnitřím nebo povrchovým zátěžím, ukládá informaci o své tloušťce v okamžiku zátěže. Tento jev je v souladu s hodnotami efektivní elastické tloušťky získanými v rámci měření flexe litosféry, a my jej zde označujeme jako "napěťová paměť materiálu". Pozornost je věnována i teoretickým základům viskoelasticity. Shrnujeme přístupy, které lze použít při formulaci konstitutivní rovnice Maxwellova typu, a důkladně analyzujeme podmínku materiálové objektivity za cílem nalezení objektivní tenzorové derivace, která odpovídá původní Maxwellově myšlence nejlépe. Zatímco těžiště práce spočívá v oblasti velkých deformací, malé deformace planetárních plášťů jsou adresovány také. Řešíme tradiční úlohu postglaciálního výzdvihu na rotující Zemi a analyzujeme změny v rotační, gravitační a elastické energii tělesa, ke kterým při tom dochází.

Contents

Introduction

The rheological behaviour of the lithosphere has long been contentious in geodynamics. The approaches developed over the years have essentially two end-members that are mutually contrasting, one treating the lithosphere as an elastic solid and the other treating it as a highly viscous fluid.

Several observations directly confirm that the surface plates constituting the lithosphere are very rigid. Many geological structures in the continental crust have survived longer than 1 Gyr without flowing away and the linearity and constant separation of transform faults proves that the oceanic plates strongly resist to any intra-plate flow. In fact, this is a fundamental postulate of plate tectonics (e.g. Turcotte & Schubert, 2002). At the same time, the lithosphere is observed to bend under imposed loads and its topography can often be fitted by the curvature of a flexed elastic plate. Thickness of such theoretical plate is referred to as the effective (or equivalent) "elastic thickness" of the lithosphere.

For this reason, modelling the lithosphere as an elastic solid has traditionally played an important role in geodynamics, particularly when response to surface loading and unloading is investigated. These flexure studies, however, also suggest that the lithosphere relaxes with time, which means that it cannot be purely elastic. It is best illustrated by the general disagreement between seismic thickness of the lithosphere, as indicated by the depth of the low-velocity zone (e.g. Shapiro & Ritzwoller, 2002), and the elastic thickness observed at long time scales, the latter being much smaller. Moreover, there is evidence for a decrease of effective elastic thickness of oceanic lithosphere with the age of imposed surface loads. An insightful review by Watts et al. (2013) employs a large dataset of topographic and gravity measurements to support and quantify these geophysical observations. In Section 0.1 of the thesis we repeat some of the conclusions presented by Watts et al. (2013) and discuss them in the context of viscoelastic rheologies.

In numerical experiments of mantle convection a different approach is taken, since convection is a phenomenon linked with fluid-like behaviour of material. The dominant type of creep mechanism in the upper and lower mantle is still debated (e.g. Ranalli, 1995; Schaeffer et al., 2016), but both major candidates – the diffusion and dislocation creep – can be described by temperature and pressure dependent viscous flow laws. For present day temperatures of terrestrial planets one obtains large viscosity contrasts with these flow laws, resulting in a mantle that convects below a highly viscous stagnant lid (Solomatov, 1995). The rheological behaviour of the outer thermal boundary layer (the lid, more generally the lithosphere) is then not of primary importance. Its internal deformation has little effect on the overall thermal evolution, layering of convection, convective vigor, the shape of plumes, or other typically addressed features.

When plastic yielding is introduced, more tectonic regimes can be obtained in thermal convection models. Namely, the mobile lid regime, similar to plate

tectonics on Earth (Tackley, 2000), and episodic lid regime, which could apply to Venus (Armann & Tackley, 2012; Rozel, 2012). Lithosphere-scale shear zones develop in these regimes due to plastic yielding, splitting the lid into plates which then subduct. Most of the deformation is accommodated within boundaries of the plates, that is, within some localized shear zones. In plate-like regimes the rheology of the lithosphere is more important, as it controls the shape of subducted slabs during their descent (e.g. Čížková et al., 2007), which in turn affects slab penetration through the transition zone (e.g. Tagawa et al., 2007), and thus also the overall convection pattern. Nevertheless, elasticity is still only rarely considered in global-scale numerical models of mobile and episodic lid regimes. In regional-scale models the behaviour of subducting slabs is under closer scrutiny and visco-elasto-plastic rheology is more common.

The basic premise of the thesis is that essentially all materials show viscoelastic properties: their short term response is elastic or elasto-brittle and when loaded for sufficient time the elastic strains are accommodated by a dissipative mechanism, gradually diminishing the stored elastic strain energy. The key question to ask is what the "sufficient time" is for a given material and given spatial scale, as recognized already by Maxwell (1871): "In the case of a viscous fluid it is time which is required, and if enough time is given, the very smallest force will produce a sensible effect, such as would require a very large force if suddenly applied. Thus a block of pitch may be so hard that you cannot make a dent in it by striking it with your knuckles; and yet it will in the course of time flatten itself by its weight, and glide downhill like a stream of water." (adopted from Málek & Rajagopal, 2005).

In the case of lithosphere the time needed for it to behave "like a stream of water" is extremely large: it can preserve elastic energy even on geological time scales, examples of which are given in Section 0.1 of the thesis. While this alone advocates for considering elasticity in mantle convection modelling, there is also another aspect. The effects of elastic deformation in regional modelling, even when short-lived, suggest a possible influence on the long-term behaviour of global-scale models. These are discussed in Section 0.2 of the thesis.

0.1 Structure and goals of the thesis

Although not discussed very often in geodynamical literature, the traditional formulation of Maxwell constitutive equation violates the principle of material frame-indifference. Every constitutive relation and other physical laws should respect this principle. The traditional formulation of Maxwell rheology is only acceptable when understood as an approximation of a more complete formulation, with its range of applicability being restricted to small strains (e.g. postglacial rebound, see below). The topic has been pioneered in the fifties by Oldroyd (1950), but is recently again gaining attention as new thermodynamics based formulations of constitutive laws are being proposed. In Chapter 1 of the thesis,

we thoroughly review the principle of material frame-indifference and bring new insights into its implications for generalizations of the traditional model.

Chapter 2 is devoted to a classical application of Maxwell rheology, in which the Earth is subject to small deformations resulting from glacial isostatic adjustment (GIA). The periodic accumulation and melting of ice loads and unloads the Earth's surface within tens to hundreds of kyr, that is, on short time scales when compared to geological processes (e.g. Peltier, 2004). Viscoelastic relaxation is crucial in explaining the postglacial rebound data. The rate at which the surface is being uplifted due to historical ice caps is an observable directly linked to the relaxation time of the lithosphere. A purely elastic Earth would predict zero present day uplift due to the already melted ice caps, because elastic models deform only when the load size is being changed. Purely viscous models, on the other hand, would predict unrealistically small uplift rates – surface loads cannot induce significant deformation of the deeper mantle when emplaced onto a non-elastic, highly viscous lithosphere. Moreover, secular drift of the rotation axis in response to GIA would be too small in a purely viscous Earth, because the readjustment of the rotational bulge would be too slow. For these reasons, a viscoelastic rheology has always been a necessity in GIA modelling, with the Maxwell model being the most common, almost unanimous, choice. Computing GIA on a rotating Earth becomes a delicate exercise as one has to account for the changes in Earth's rotation induced by the load induced deformation. In Section 2.2 of the thesis we analyze this phenomena from an energetic point of view. We derive a diagnostic tool that can be used, within the field of small planetary deformations, to detect physically ill-posed problems, or to reveal numerically incorrect solutions to physically well-posed problems. We apply this tool to review the approximations commonly used in GIA modelling and demonstrate some of their inconsistencies.

The main goal of the thesis is to investigate the footprints of viscoelasticity in the context of mantle convection. We study how elasticity influences the surface topography and lithospheric stresses when internal loading is generated by self-consistently developed plumes and downwellings. The focus is on mantle-lithosphere interaction: how the internal dynamics impacts the deformation of a viscoelastic lithosphere and, conversely, how the elastic properties of the lithosphere affect the internal dynamics. In Chapter 2, we evaluate the response of a stagnant lid and discuss the importance of the lid thickness and its evolution in time. We perform simulations of a model Mars that is cooling down from its initially hot state and analyze the stress patterns in its thickening lithosphere. Statistically steady state, in which the lid thickness remains constant in time, is also addressed. In Chapter 4 of the thesis, we study the transition from a stagnant lid to plate-like mode of convection in visco-elasto-plastic models. We asses the fluctuations of lithospheric stresses that are associated with the chaotic movement of sinking and rising plumes and explore whether the expected effects of elasticity and a free surface emerge despite these fluctuations.

1. Small deformations of a viscoelastic mantle

1.1 Eulerian formulation of the governing equations

Throughout the thesis we use Eulerian description of field variables, meaning that the domain of these variables is the current configuration of the body at time t. Such an approach is typical when mantle convection is addressed, see Chapters 3 and 4 of the thesis, but it is not very common when small deformations of a planet, for example caused by surface loads, are being computed. In this case it is more common to use Lagrangian description of field variables, with their domain being some convenient reference configuration that has a regular shape. The advantage is that a symmetrical domain allows for the use of fast numerical methods – in planetary science it is often assumed to be a sphere or spherical shell, allowing the use of so-called spectral methods (decomposing field variables into spherical harmonics).

In Section 1.2, dealing with deformation of the Earth due to surface glaciers and rotation, we use the Eulerian description of variables, but still choose the computational domain to be a time constant spherical shell. This somewhat puzzling combination enables us to harvest the elegance intrinsic to the Eulerian formulation – the absence of any additional terms related to the fact that in the Lagrangian formulation the body forces are expressed at locations where they do not actually act – and at the same time to employ a spectral method. The approach has appeared in geodynamical literature several times in the past decade (e.g. Tobie et al., 2008; Golle et al., 2012; Souček et al., 2016), but the papers are mostly application driven. We carefully derive the governing equations in this section in order to avoid any potential confusions.

Let us assume a spherical body at rest, its static pressure p_0 counteracting the gravitational forcing $\rho\boldsymbol{g}_0$, ρ being the density and $\boldsymbol{g}_0$ the gravitational acceleration (see the left panel of Fig. 1.1). When the body is subject to a conservative forcing described by potential ζ it deforms. Eulerian formulation of the equation of motion then reads

$$\nabla \cdot \boldsymbol{\tau} + \rho\boldsymbol{g}_0 - \rho\nabla\zeta = 0 \quad \text{in} \quad v(t), \tag{1.1}$$

where $\boldsymbol{\tau}$ is the Cauchy stress tensor and ζ is the potential driving deformation (e.g. centrifugal potential or perturbation of the gravitational potential due to the change of the body's shape – see Section 1.2). Eq. (1.1) is valid within the deformed body occupying the region $v(t)$. If the surface of the body is free, the

boundary condition reads

$$\boldsymbol{\tau} \cdot \boldsymbol{n} = 0 \quad \text{on} \quad s^- \cap s^+, \tag{1.2}$$

where $\boldsymbol{n}$ is the outer normal vector to surfaces s^- and s^+ of the deformed body, depicted on the right panel of Fig. 1.1. If the body's deformation is driven by surface loads, the boundary condition (1.2) is replaced with $\boldsymbol{\tau} \cdot \boldsymbol{n} = (\boldsymbol{g}_0 + \nabla\zeta)\,\sigma^{\mathrm{L}}$, σ^{L} representing surface mass density of the load. In this section we further assume $\sigma^{\mathrm{L}} = 0$ for clarity. Systems described by eq. (1.1) are often referred to as hydrostatically pre-stressed bodies. The effect of the static pressure p_0, which satisfies

$$-\nabla p_0 + \rho \boldsymbol{g}_0 = 0 \quad \text{in} \quad S_0 \tag{1.3}$$

and is equal to zero elsewhere, can be subtracted by subtracting eq. (1.3) from eq. (1.1). The governing equations (1.1) and (1.2) then take the form

$$\nabla \cdot \bar{\boldsymbol{\tau}} - \rho\nabla\zeta = 0 \quad \text{in} \quad v^{\mathrm{J}}(t), \tag{1.4}$$

$$\nabla \cdot \bar{\boldsymbol{\tau}} + \rho\boldsymbol{g}_0 - \rho\nabla\zeta = 0 \quad \text{in} \quad v^{+}(t), \tag{1.5}$$

$$\bar{\boldsymbol{\tau}} \cdot \boldsymbol{n} = p_0 \boldsymbol{n} \quad \text{on} \quad s^{-}(t), \tag{1.6}$$

$$\bar{\boldsymbol{\tau}} \cdot \boldsymbol{n} = 0 \quad \text{on} \quad s^{+}(t), \tag{1.7}$$

where $\bar{\boldsymbol{\tau}} := \boldsymbol{\tau} + p_0\mathcal{I}$, $\mathcal{I}$ being the identity tensor. Note that the static pressure p_0 is defined by eq. 1.3 as a positive quantity inside the sphere S_0 and zero outside that sphere. In Section 1.2 we solve, however, the following set of equations:

$$\nabla \cdot \bar{\boldsymbol{\tau}} - \rho\nabla\zeta = 0 \quad \text{in} \quad S_0, \tag{1.8}$$

$$\bar{\boldsymbol{\tau}} \cdot \boldsymbol{n} = u_r \rho \boldsymbol{g}_0 \quad \text{on} \quad \partial S_0, \tag{1.9}$$

where $\boldsymbol{e}_r$ is the outer normal to surface ∂S_0 and u_r is the radial component of the Eulerian displacement field $\boldsymbol{u}$.

To show that eqs (1.8)–(1.9) are a reasonable approximation of the original eqs (1.1)–(1.2), resp. of their equivalent eqs (1.4)–(1.7), we investigate the terms (1.5) and (1.6). Upon integrating (1.5) over the volume $v^+(t)$ and using the Gauss theorem, together with the free surface condition (1.7), we get

$$-\int_{\partial S_0^+} \bar{\boldsymbol{\tau}} \cdot \boldsymbol{e}_r \,\mathrm{d}s + \int_{v^+(t)} \rho(\boldsymbol{g}_0 - \nabla\zeta)\,\mathrm{d}v = 0. \tag{1.10}$$

The second term in eq. (1.10) can be subject to a series of approximations:

$$\int_{v^+(t)} \rho(\boldsymbol{g}_0 - \nabla\zeta)\,\mathrm{d}v \cong \int_{v^+(t)} \rho\boldsymbol{g}_0\,\mathrm{d}v \cong \int_{\partial S_0^+} \rho\boldsymbol{g}_0\, u_r\,\mathrm{d}s, \tag{1.11}$$

where we first assumed $\nabla\zeta \ll \boldsymbol{g}_0$ and then we expressed the volume element $\mathrm{d}v$ of $v^+(t)$ as $u_r\,\mathrm{d}s$. Note that the second step is approximative for two reasons: 1)

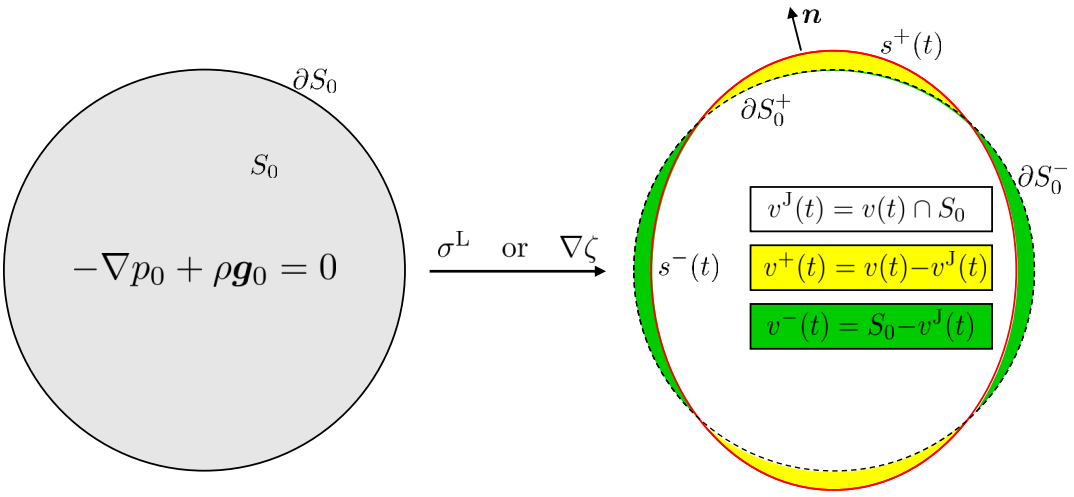

Figure 1.1: A sphere S_0 deforms and becomes volume $v(t)$ due to the acting of a surface load σ^{L} or due to a disturbing potential ζ. The surface ∂S_0 can be separated into the part ∂S_0^+ which goes up and becomes s^+ after the deformation. The other part, ∂S_0^-, descends and becomes s^- after the deformation.

radial variations of the integrand, $\rho \boldsymbol{g}_0$, within the volume $v^+(t)$ are neglected, and 2) the height of topography above the sphere S_0 is estimated by the value of u_r at the surface ∂S_0^+ and not at the surface s^+. Since we use Eulerian description of variables, the displacement field $\boldsymbol{u}$ taken at ∂S_0^+ represents the displacement of material particles that are at ∂S_0^+ after the deformation. It is thus only a first-order estimate of the actual topography height, which is equal to the value of u_r taken at the surface of the deformed body s^+. Eq. (1.11) together with eq. (1.10) yield

$$\int_{\partial S_0^+} (-\bar{\boldsymbol{\tau}} \cdot \boldsymbol{e}_r + \rho \boldsymbol{g}_0 \, u_r) \, \mathrm{d}s \cong 0, \tag{1.12}$$

which is the boundary condition (1.9) on ∂S_0^+. In other words, the volumetric force $\rho(\boldsymbol{g}_0 - \nabla\zeta)$ was found dynamically equivalent to the surface traction $\rho \boldsymbol{g}_0 \, u_r$, acting at the spherical surface ∂S_0^+. Also note that the approximation $\nabla\zeta \ll \boldsymbol{g}_0$ could be easily avoided by replacing $\boldsymbol{g}_0$ with $(\boldsymbol{g}_0 - \nabla\zeta)$ in eq. (1.9).

For regions with negative topography we integrate the traction in eq. (1.6) over the surface $s^-(t)$,

$$\int_{s^-(t)} p_0 \boldsymbol{n} \, \mathrm{d}s \cong \int_{s^-(t)} -\rho g_0 u_r \, \boldsymbol{n} \mathrm{d}s \cong \int_{\partial S_0^-} \rho \boldsymbol{g}_0 u_r \, \mathrm{d}s \,, \tag{1.13}$$

where in the first step the static pressure p_0 at the surface $s^-(t)$ was set equal to $-\rho g_0 u_r$, which neglects the radial variations of ρg_0 within the volume $v^-(t)$, similarly as in eq. (1.11). In the second step the surface element $\boldsymbol{n}\mathrm{d}s$ of $s^-(t)$ was approximated by the surface element of ∂S_0^-, which is a good first-order estimate. Observing eq. (1.13) directly shows that the boundary traction (1.6) is dynamically analogous to the prescribed traction (1.9) on ∂S_0^-, concluding the correspondence of eqs (1.8)–(1.9) with the set (1.4)–(1.7).

Instead of the procedure above, the same conclusions can be reached by performing the Taylor expansion of (1.2), as done in appendix to Souček et al. (2016):

$$0 = \boldsymbol{\tau}(\boldsymbol{r}_\mathrm{s}+\boldsymbol{u}) \cdot \boldsymbol{n}(\boldsymbol{r}_\mathrm{s}+\boldsymbol{u}) = (\bar{\boldsymbol{\tau}} - p_0\mathcal{I})(\boldsymbol{r}_\mathrm{s}+\boldsymbol{u}) \cdot \boldsymbol{n}(\boldsymbol{r}_\mathrm{s}+\boldsymbol{u}) \tag{1.14}$$

$$\cong \boldsymbol{n}p_0(\boldsymbol{r}_\mathrm{s}) + \bar{\boldsymbol{\tau}}(\boldsymbol{r}_\mathrm{s}) \cdot \boldsymbol{n} + \boldsymbol{u} \cdot [\nabla(p_0\boldsymbol{n})]_{\mathrm{r=r_s}} + \boldsymbol{u} \cdot [\nabla(\bar{\boldsymbol{\tau}} \cdot \boldsymbol{n})]_{\mathrm{r=r_s}} \tag{1.15}$$

$$\cong \bar{\boldsymbol{\tau}}(\boldsymbol{r}_\mathrm{s}) \cdot \boldsymbol{e}_r + \rho g_0 u_r(\boldsymbol{r}_\mathrm{s})\boldsymbol{e}_r \tag{1.16}$$

where $\boldsymbol{r}_\mathrm{s}$ is the position vector tracking the spherical surface ∂S_0, $p_0(\boldsymbol{r}_\mathrm{s})$ was recognized as zero, the normal vector $\boldsymbol{n}$ was approximated by $\boldsymbol{e}_r$, the term $\boldsymbol{u}\cdot[\nabla(p_0\boldsymbol{n})]_{\mathrm{r=r_s}}$ was approximated by $\rho g_0 u_r(\boldsymbol{r}_\mathrm{s})\boldsymbol{e}_r$, and the last term on the second line was neglected. We believe, however, that the more detailed analysis provided here may help the reader in understanding the derivations in Section 2.2 of the thesis.

The following section is an excerpt from a publication in Geophysical Journal International, Volume 212(2), p. 955-975, doi: 10.1093/gji/ggx469, 2017.

1.2 Energy balance of GIA on a rotating Earth

Understanding the feedback between glacial isostatic adjustment (GIA) and the Earth's rotation is important for an accurate prediction of sea level changes induced by climate and tectonic processes. Here we consider a simple, four-layer incompressible Earth model, recently used for a benchmark of GIA codes, to estimate the accuracy of the linearized Liouville equation (LE) and to demonstrate that models with an incomplete or missing rotational feedback violate the principle of energy conservation. First, we compute GIA on a rotating Earth by solving the equation of motion coupled with LE in its full nonlinear form. By comparing the nonlinear LE solution with the traditional linearized one, we find that the radial component of the angular velocity vector is inaccurate in the latter case, with an error exceeding 10% already after 1 kyr of evolution. To understand the cause of this discrepancy, we investigate the time evolution of different kinds of energy involved in the process. While the rotational, elastic and dissipative energies are straightforward to compute, the formula for the gravitational energy contains an integral that requires a careful, higher-order accurate evaluation of the gravitational potential perturbation. We circumvent this problem by transforming the integral into a different one, formulated in terms of displacement instead of potential. We find that the solution of the linearized LE equation does not conserve the energy, since, in the linearized case, the rate of change of the rotational energy is not equal to the power of the centrifugal force. We also compute the energy balance of GIA on a constantly rotating Earth, and demonstrate the importance of the rotational feedback in the equation of motion. The formalism derived in this study allows a detailed examination of the energy balance for

a rotating, incompressible planetary body deformed by a surface load. As such, it may not only serve as a reliable tool for *a posteriori* testing of GIA numerical solutions but it can also be used in different planetary science applications.

1.2.1 Selected results

In this section we analyze the temporal evolution of the gravitational, rotational, elastic, and dissipative energy of a model Earth whose shallow layers are being deformed by post-glacial rebound and whose rotation is changing in response to this process. The setting of our numerical experiment corresponds to the benchmark case adopted from Spada et al. (2011), the details of which are discussed in Section 2.2.3 of the thesis. The rotating Earth model M3-L70-V01, initially in equilibrium state, is suddenly loaded with a spherical ice cap. The loading and the associated deformation induce a polar motion (PM) (Fig. 2.3a of the thesis) and changes in the rotational speed (Fig. 2.3b of the thesis), which are accompanied by large variations in the rotational and gravitational energy (Fig. 1.2, red and green curves, respectively). The amplitudes of these variations are of the order of $10^{22} - 10^{23}$ J and they are three orders of magnitude larger than the variations in the elastic (magenta) and dissipative (blue) energy (cf. also Figs 2.5 and 2.6 of the thesis). During the whole evolution, the sum of all energies is constant (full black line).

So far we have discussed the results computed using the NLE. In Fig. 1.2 the variations of the gravitational and rotational energy obtained using the LLE are shown by dashed and dotted black lines, respectively. While the curve for the gravitational energy coincides almost exactly with that obtained using the NLE, the accuracy in determining the rotational energy decreases with increasing time, resulting in a relative error of almost 100% after 5 kyr. Consequently, the total energy of the system (dashed black line) is not conserved for the LLE solution.

As demonstrated in Fig. 1.3a, the large error in evaluating the rotational energy is associated with determining the component m_3, which is significantly larger than the value obtained using the NLE, in contrast to components m_1 and m_2, which are determined with high accuracy (see Fig. 2.3a of the thesis). Figure 1.3b shows that the predicted degree 2 shape of the Earth does not depend on whether we use the NLE or LLE, suggesting that the displacement obtained using the LLE is only slightly affected by the error in m_3. This explains the good agreement obtained for the gravitational energy which is a function of the radial component of displacement (see eq. 2.52 of the thesis) and, unlike the rotational energy, does not depend directly on m_3.

Note that the difference between the NLE and LLE solution for m_3 is not related to the free wobble, as illustrated by the green line in Fig. 1.3a. The line represents a case in which the ice cap is being imposed only gradually onto the surface of the Earth, over the period of 5 yr, significantly reducing the amplitude of the induced wobble but leading to the same long term behaviour as for the

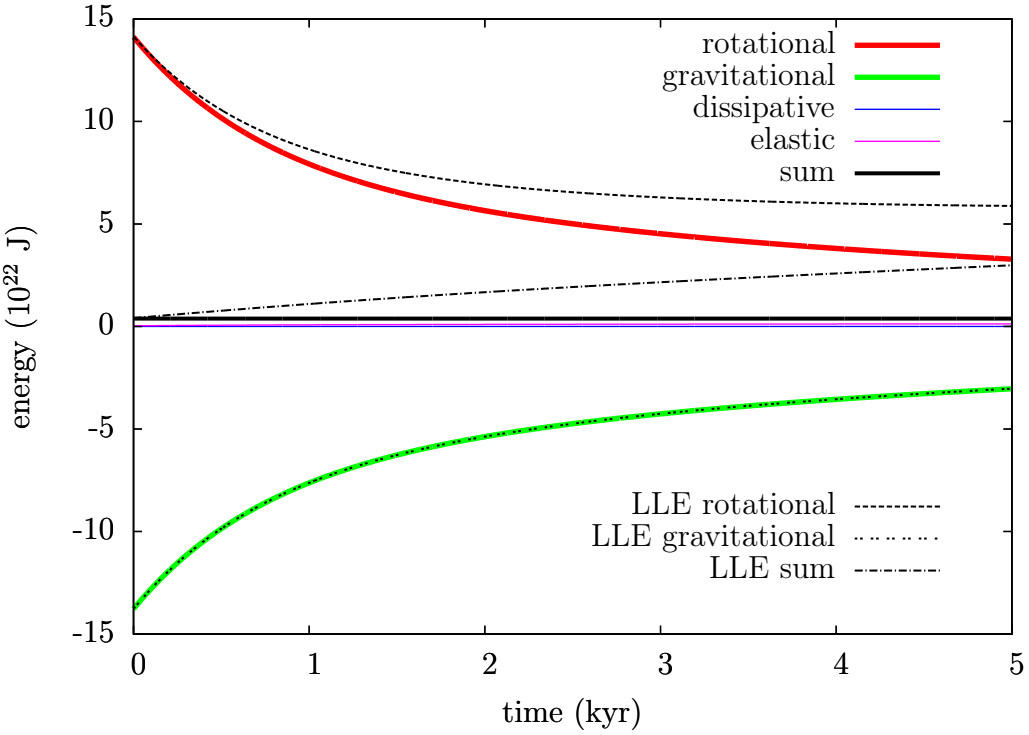

Figure 1.2: Time evolution of different types of energy for rotating model M3-L70-V01 loaded with an ice cap at t=0 (for details, see Spada et al., 2011). The variations of energy are plotted with respect to the initial equilibrium state in which the rotational vector is parallel to the main axis of the body. The results obtained using the NLE are represented by coloured lines while the LLE solution is plotted in black.

instantaneous loading.

In the light of the results presented in Section 2.2.3 of the thesis, the large error in component m_3 obtained using the LLE may be viewed as surprising. As demonstrated in Fig. 2.3b of the thesis, both the NLE and LLE predict the same LOD variation ΔLOD given by eq. (2.33) of the thesis (right), but m_3 computed as $m_3 = -c_{33}/C$ is still significantly affected by the neglect of the nonlinear terms in the LE (Fig. 1.3a). To explain this apparent paradox, we start from the formula (9.2.3) in Munk & MacDonald (1960)

$$\frac{\Delta\mathrm{LOD}}{\mathrm{LOD}} = -m_3 = \frac{c_{33}}{C}\,, \tag{1.17}$$

and we describe the simplifications that were used in its derivation. The first equality in eq. (1.17) can be derived by linearization of the exact formula for ΔLOD:

$$\frac{\Delta\mathrm{LOD}}{\mathrm{LOD}} = \frac{2\pi\omega^{-1} - 2\pi\omega_0^{-1}}{2\pi\omega_0^{-1}} = \frac{\omega_0 - \omega}{\omega} \cong \frac{\omega_0 - \omega}{\omega_0} = 1 - \sqrt{m_1^2 + m_2^2 + (1+m_3)^2}\,. \tag{1.18}$$

Using the binomial theorem and neglecting the higher-order terms, we obtain

$$\frac{\Delta\mathrm{LOD}}{\mathrm{LOD}} \cong -m_3 + \tfrac{1}{2}\left(m_1^2 + m_2^2 + m_3^2\right)\,, \tag{1.19}$$

which, after neglecting the quadratic terms, gives the first equality in eq. (1.17). The second equality in eq. (1.17) comes from the LLE for component m_3. In Appendix A of the thesis we derive the following higher-order approximation:

$$-m_3 + \frac{1}{2}(m_1^2 + m_2^2 + m_3^2) \cong \frac{c_{33}}{C}\,. \tag{1.20}$$

Combining eq. (1.20) with eq. (1.19) yields a more accurate version of the original equation (1.17):

$$\frac{\Delta\mathrm{LOD}}{\mathrm{LOD}} \cong -m_3 + \frac{1}{2}(m_1^2 + m_2^2 + m_3^2) \cong \frac{c_{33}}{C}\,. \tag{1.21}$$

The definition of ΔLOD in eq. (2.33) of the thesis thus includes second-order accurate evaluation of the LOD variation, while the equation $m_3 = -c_{33}/C$ is only first-order accurate, which explains the disagreement between the LLE and NLE solutions in Fig. 1.3a.

The fact that the m_3 component of the rotation vector is affected by a large error does not invalidate the results of previous studies using the LLE solution. As demonstrated above, the traditional equation for $\triangle$LOD that is used in these studies is more accurate than the linearized equation for m_3, and it gives the same LOD variation as the NLE equation (Fig. 2.3b of the thesis), provided that excursions of the rotation axis are small.

Our numerical tests (not presented in this paper) suggest that the shift of the

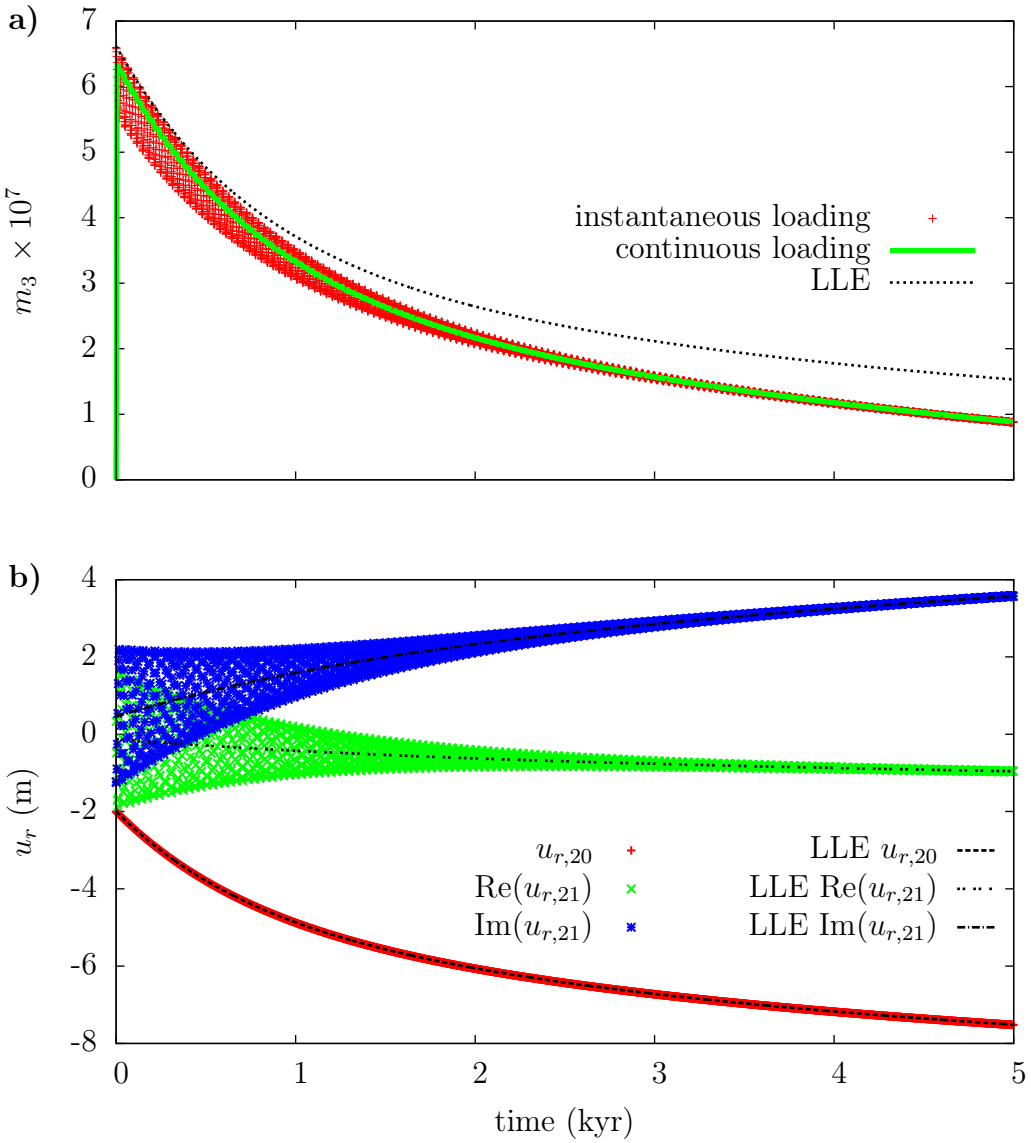

Figure 1.3: a) Time evolution of m_3 for the studied benchmark case (cf. Fig. 2.3 of the thesis). Red points depict our NLE solution, dashed line is the LLE solution. Green line shows our solution when the spherical ice cap is imposed on the surface of the Earth only gradually (over the period of 5 yr). b) Displacement components $u_{r,20}$ and $u_{r,21}$ relative to the hydrostatic equilibrium for the same case as above (continuous loading is omitted for clarity of the figure).

rotation axis must be larger than 1 degree for the nonlinearity to significantly (by at least a few percent) affect the resulting PM and LOD. The ice cap considered here is rather small and, since the characteristic time of equatorial bulge readjustment is inversely proportional to the size of the load (Ricard et al., 1993), several Myr would be needed to shift the pole by 1 degree. If we considered an unrealistic, ten times larger ice cap, the equatorial bulge readjustment would occur faster and the linearized PM and LOD solutions would differ from the nonlinear one by few percent already after about 200 kyr.

The following chapter is an excerpt from a publication in Geophysical Journal International, Volume 209(3), p. 1462-1475, doi: 10.1093/gji/ggx102, 2017

2. Stress memory effect in viscoelastic stagnant lid convection

Present thermo-chemical convection models of planetary evolution often assume a purely viscous or visco-plastic rheology. Ignoring elasticity in the cold, outer boundary layer is, however, questionable since elastic effects may play an important role there and affect surface topography as well as the stress distribution within the stiff cold lithosphere. Here we present a modelling study focused on the combined effects of Maxwell viscoelastic rheology and a free surface in the stagnant lid planetary convection. We implemented viscoelastic rheology in the StagYY code using a tracer-based stress advection scheme that suppresses subgrid oscillations. We apply this code to perform thermal convection models of the cooling planetary mantles and we demonstrate that while the global characteristics of the mantle flow do not change significantly when including viscoelasticity, the stress state of the cold lithosphere may be substantially different. Transient cooling of an initially thin upper thermal boundary layer results in a complex layered stress structure due to the memory effects of viscoelastic rheology. The stress state of the lid may thus contain a record of the planetary thermal evolution.

2.1 Governing equations and numerical methods

We employ two types of models. First, we perform models of purely composition driven convection with a simple density load (labeled as RC). A compositionally buoyant cylinder represents a rising plume head and we evaluate the effects of elasticity and surface boundary condition on the topography. In the second group of numerical experiments (labeled TC) we use viscoelastic thermal convection models and concentrate on the stress evolution within the lithosphere.

2.1.1 Governing equations

We assume an incompressible fluid with infinite Prandtl number with following equations describing conservation of mass and momentum:

$$\nabla \cdot \boldsymbol{v} = 0, \tag{2.1}$$

$$-\nabla p + \nabla \cdot \boldsymbol{\tau} + \rho \boldsymbol{g} = 0. \tag{2.2}$$

Here $\boldsymbol{v}$ is the velocity, ρ density, p pressure, $\boldsymbol{g}$ gravitational acceleration and $\boldsymbol{\tau}$ deviatoric stress. In case of the compositional models (RC) we further require the conservation of composition:

$$\frac{\partial c_k}{\partial t} + \boldsymbol{v} \cdot \nabla c_k = 0, \tag{2.3}$$

where c_k is the concentration (either 0 or 1) of kth material with the density ρ_k.

In the thermal convection models (TC), eqs (2.1) and (2.2) are supplemented by conservation of energy in the Boussinesq approximation:

$$\frac{\partial T}{\partial t} = \kappa \triangle T - \boldsymbol{v} \cdot \nabla T, \tag{2.4}$$

and a linearized equation of state:

$$\rho = \rho_0 (1 - \alpha (T - T_0)). \tag{2.5}$$

where T is the temperature, κ is the diffusivity, α is the thermal expansivity and ρ_0 is the density at reference temperature T_0. Both thermal expansivity and diffusivity are assumed constant.

2.1.2 Maxwell viscoelastic rheology

The rheological description of a Maxwell viscoelastic material is given by

$$\mathbb{D} = \mathbb{D}_{\text{viscous}} + \mathbb{D}_{\text{elastic}} = \frac{1}{2\eta(p_0, T)} \boldsymbol{\tau} + \frac{1}{2G} \frac{\mathcal{D}\boldsymbol{\tau}}{\mathcal{D}t}, \tag{2.6}$$

where $\mathbb{D}$ is the deviatoric part of the strain rate tensor, $\eta(p_0, T)$ is the viscosity dependent on temperature and hydrostatic pressure p_0, and G is the shear modulus. $\frac{\mathcal{D}}{\mathcal{D}t}$ denotes an objective tensor rate (e.g. Liu & Sampaio (2014)). Here we adopt the Jaumann rate that is traditionally used in viscoelastic convection (see appendix A in Thielmann et al. (2015) and Muhlhaus & Regenauer-Lieb (2005) for a discussion of objective rates in geodynamical context):

$$\frac{\mathcal{D}\boldsymbol{\tau}}{\mathcal{D}t} := \frac{\partial \boldsymbol{\tau}}{\partial t} + \boldsymbol{v} \cdot \nabla \boldsymbol{\tau} + (\boldsymbol{\tau}\mathbb{W} - \mathbb{W}\boldsymbol{\tau}), \tag{2.7}$$

where $\mathbb{W}$ is the antisymmetric part of the velocity gradient (spin tensor)

$$\mathbb{W} = \frac{1}{2} \left(\nabla \boldsymbol{v} - (\nabla \boldsymbol{v})^{\mathrm{T}} \right). \tag{2.8}$$

The corotational term $(\boldsymbol{\tau}\mathbb{W} - \mathbb{W}\boldsymbol{\tau})$ accounts for rotation of a volume element within the flow. Inserting (2.7) into (2.6) gives the following form of the constitutive equation:

$$2\eta\mathbb{D} = \boldsymbol{\tau} + \frac{\eta}{G} \left(\frac{\partial \boldsymbol{\tau}}{\partial t} + \boldsymbol{v} \cdot \nabla \boldsymbol{\tau} + \boldsymbol{\tau}\mathbb{W} - \mathbb{W}\boldsymbol{\tau} \right). \tag{2.9}$$

We consider an Arrhenius viscosity that depends exponentially on temperature and hydrostatic pressure p_0:

$$\eta(p_0, T) = \eta_0 \cdot \exp \left(\frac{E_{\text{act}} + p_0 V_{\text{act}}}{RT} \right), \tag{2.10}$$

where η_0 is set such that η is the reference viscosity at $T = 1600$ K and $p_0 = 0$ Pa, $E_{\rm act}$ is the activation energy, $V_{\rm act}$ is the activation volume and R is the gas constant. In viscous models that will be used as a reference to evaluate elasticity effects, $G \to \infty$ in Eq. (2.9) and viscosity follows the same pressure and temperature dependency (Eq. (2.10)).

Following Moresi et al. (2002) we discretize Eq. (2.9) with a mixed Euler first-order accurate scheme (implicit with respect to $\mathbb{D}$, $\boldsymbol{\tau}$ and viscosity, explicit with respect to advectional and corotational terms) and obtain the equation for stress in the nth time step:

$$\boldsymbol{\tau}^{\rm n} = 2{\rm Z}\eta\mathbb{D}^{\rm n} + (1-{\rm Z})\tilde{\boldsymbol{\tau}}^{\rm n-1}, \tag{2.11}$$

$$\tilde{\boldsymbol{\tau}}^{\rm n-1} := \boldsymbol{\tau}^{\rm n-1} - \triangle t\left(\boldsymbol{v}\cdot\nabla\boldsymbol{\tau} + \boldsymbol{\tau}\mathbb{W} - \mathbb{W}\boldsymbol{\tau}\right)^{\rm n-1}, \tag{2.12}$$

$${\rm Z} = \frac{\triangle t}{\triangle t + \eta/G}\,. \tag{2.13}$$

The implementation of viscoelasticity into a viscous flow code thus consists of replacing viscosity by numerical viscosity $\eta_{\rm num} := {\rm Z}\eta$ and evaluating an extra term $\nabla\cdot[(1-{\rm Z})\tilde{\boldsymbol{\tau}}^{\rm n-1}]$, which accounts for the effect of stress that did not fully relax within one time step. The importance of elastic effects is measured by viscoelasticity parameter Z that is closely related to the Maxwell relaxation time $t_{\rm M} = \eta/G$ (${\rm Z}\to 1$ when $\eta/G \ll \triangle t$). In nondimensional studies, the role of $t_{\rm M}$ is played by the Deborah number, $De := \eta\kappa G^{-1}D^{-2}$, with D denoting the domain's depth.

Let us consider a constant value of the shear modulus, $G = 7\cdot 10^{10}$ Pa (representative of the Earth's uppermost mantle). Then, for viscosity (in the mantle) equal to 10^{22} Pa s the relaxation time η/G is ~ 4.5 kyr. With a typical computational time step of 100 kyr more than 95% of stress is relaxed within one time step and the material behaves effectively as a viscous fluid. However, if the viscosity (in the lithosphere) is $\eta = 10^{27}$ Pa s, the relaxation time is ~ 450 Myr and for the same computational time step only 0.02% of stress is relaxed within one time step. Consequently, the material remembers its stress state from thousands of previous time steps.

In order to evaluate the differences between different viscous and viscoelastic models we introduce a scalar measure of stress, the second invariant of the stress tensor, which we will refer to as the effective stress:

$$\tau_{\rm eff} := \sqrt{\frac{\tau_{xx}^2 + \tau_{zz}^2}{2} + \tau_{xz}^2}\,, \tag{2.14}$$

with τ_{xx}, τ_{zz} and τ_{xz} denoting the Cartesian components of $\boldsymbol{\tau}$.

Time derivative of $\boldsymbol{\tau}$ in Eq. (2.9) implies the need for an initial condition on the deviatoric stress. In all viscoelastic models we assume $\boldsymbol{\tau}(t=0)$ equal to zero.

2.2 Thermal convection (TC models)

2.2.1 Model setup

In Section 3.3 of the thesis we examined the basic characteristics of a viscoelastic response in free-slip and free-surface models of a cylinder rising below a stiff lid. Now we proceed towards mantle convection models, in which the flow is driven by thermal buoyancy and the viscosity is controlled by the temperature distribution and the depth.

We concentrate on the effects of viscoelasticity on the transient behaviour of the stiff lid and demonstrate how viscoelasticity affects stress evolution in the lithosphere during its cooling and thickening. To that end we perform models of two planetary bodies with different reference viscosities and thus different vigour of convection in the transient phase. The first one is an Earth-sized body (E-models) with a relatively high η_{ref} and model parameters based on Crameri & Tackley (2014). The other one is a Mars-sized body (M-models) with lower η_{ref} and parameters taken from Golle et al. (2012). For each planet we test two scenarios – one with an initially thin lithosphere (controlled by the initial thermal boundary layer thickness $d_{\mathrm{TB}} = 30$ km) and the other one with an initially 300 km thick lithosphere.

We assume basally heated convection with constant temperature top and bottom boundaries, while the sides are insulating with zero normal heat flux. The initial temperature distribution follows the relation:

$$T(z) = T_0 + (T_{\mathrm{surf}} - T_0) \exp\left(\frac{-z}{d_{\mathrm{TB}}}\right) + (T_{\mathrm{CMB}} - T_0) \exp\left(\frac{z - D}{d_{\mathrm{TB}}}\right), \qquad (2.15)$$

where $T_0 = 1900$ K is the temperature at the mid-depth, T_{surf} and T_{CMB} are surface and core-mantle boundary temperatures, d_{TB} is the initial thickness of the thermal boundary layer, D is the mantle thickness and z is the depth. Random temperature perturbations with amplitude 20 K are used to initiate convection. The model parameters are summarized in Table 2.1.

Each convection simulation starts with a transient stage in which the sublithospheric flow evolves and the cold, stiff lithosphere gradually changes its thickness. Then, a statistically steady state is reached and the lithospheric thickness remains constant. The temperature T_0 in the mid-mantle is initially set to 1900 K. For E-models this is less than the statistically steady state mid-mantle temperature, thus the central part of the model heats up during transient phase and the vigour of convection increases. For the Mars-like parameter set, on the other hand, 1900 K represents an overheated mantle, mainly because of the smaller temperature drop between the core-mantle boundary and surface. Due to the lower reference viscosity, a vigorous, downwelling dominated convection initially develops in the model and is gradually quelled as the mid-mantle temperature decreases down to cca. 1700 K.

Table 2.1: Parameters used in the convection calculations

Parameter	Symbol	Model E_{el}	Model M_{el}	Units
Mantle depth	D	2890	1666	km
Gravitational acceleration	g	9.81	3.7	m s^{-2}
Reference density	ρ_0	3300	3300	kg m^{-3}
Temperature drop	$\triangle T$	2500	1500	K
Reference viscosity	η_{ref}	10^{23}	$9.316 \cdot 10^{19}$	Pa s
Upper viscosity cut-off	η_{max}	10^{28}	10^{28}	Pa s
Thermal diffusivity	κ	$7.6 \cdot 10^{-7}$	$7.6 \cdot 10^{-7}$	m^2 s^{-1}
Thermal expansivity	α	$3 \cdot 10^{-5}$	$3 \cdot 10^{-5}$	K^{-1}
Activation energy	E_{act}	240	346	kJ mol^{-1}
Activation volume	V_{act}	$8.9 \cdot 10^{-7}$	$2 \cdot 10^{-7}$	m^3 mol
Surface temperature	T_{surf}	289	230	K
Shear modulus[a]	G	$7 \cdot 10^{10}$	$7 \cdot 10^{10}$	Pa

[a]Models E_{vis} and M_{vis} are obtained by setting $G \to \infty$

The model domain is a 2-D Cartesian box with aspect ratio 1 and a mantle depth of 2890 km for E-models and 1666 km for M-models. Impermeable free slip boundaries are assumed at the bottom and sides of the box. The top boundary is either assumed to be impermeable free slip, or similarly to the RC models, a free surface using the sticky-air approach. Following Crameri & Tackley (2014) we use a 150 km thick sticky-air layer with viscosity $\eta_{\mathrm{A}} = 10^{21}$ Pa s (given our upper viscosity cut-off, this choice provides a reasonable balance between obtained accuracy and the length of computational time step necessary to avoid the "drunken seaman" instability described by Kaus et al. (2010) and Duretz et al. (2011)). The mesh resolution is 256×256 nodes.

2.2.2 Results: free surface

In Section 3.4.2 of the thesis we described the results of convection models with a free-slip surface. Now let us focus on the models with a free surface. Based on the results of our numerical experiments with a rising cylinder, we may expect much stronger effects of elasticity, as the lithospheric flexure can now fully develop.

Fig. 2.1 shows the stress evolution in the smaller Mars-like mantle models M_{vis} and M_{el} – with initially thin lithosphere $d_{\mathrm{TB}} = 30$ km. In a purely viscous model (left column) the stress pattern in the lithosphere reflects its bending due to the pull of the sublithospheric downwellings (no plumes are initially present due to the fact that the mantle is overheated). The wavelength of the lithospheric undulations is controlled by the temporary distribution of the downwellings and by the actual thickness of the lithosphere. As the lithosphere cools and thickens, the wavelength of the undulations generally increases. In a viscoelastic case (right column) the stress pattern is again much more complex. Stresses obtained during the bending of initially thin plate (easy to bend and thus reaching relatively large strains) are remembered ('frozen') until cca. 4 Gyr and during cooling and thickening of the lid its deeper parts adopt and remember the stresses due to

later bending. The amplitude of the stress in the deeper layers is smaller than the amplitude of the initial surface stress layer due to the fact that the colder and thicker lid becomes increasingly difficult to bend. These large stresses are preserved on time scales comparable to the surface value of t_{M} (4.5 Gyr). After 3 Gyr mantle has cooled down enough and plumes start to develop. Large stresses associated with strong plumes pushing at the base of the lithosphere then overprint the stress pattern associated with the cooling and early bending. Note that the lithospheres of the models with a free surface exhibit bending stresses that are order of magnitude larger than in the previously discussed simulations with a free slip upper boundary.

Figure 2.2 shows vertical profiles of effective stress (horizontally averaged) in both models $\mathrm{M_{vis}}$ and $\mathrm{M_{el}}$, evenly sampled over the first 3 Gyr. It demonstrates thickening of the viscous lithosphere with a typical bending/unbending pattern (left panel) while the viscoelastic lithosphere with generally lower stresses shows preservation of the bending pattern of the initially thin lithosphere (right panel). Note that the stresses associated with bending of the 30 km thick lithosphere are in tens of MPa, while we observed stresses of only a few MPa in the free-slip surface simulations. In the viscoelastic model, the stresses below the 30 km depth are similar as in the free-slip case.

After examining the effects of lithospheric thickening, let us now look at the models in which the lithosphere is initially thick ($d_{\mathrm{TB}} = 300$ km). Such models display no differences between viscous and viscoelastic rheology, in case that a free slip condition is prescribed at the top (Section 3.4.2 of the thesis). In free surface models we do observe differences, but of a different nature than the stress memory effect described above.

In these models, the lithosphere is thinning and the layered stress structures thus could not develop here. The stress patterns are dominated by the bending stresses, and these are significantly smaller for the viscoelastic simulations (see the last paragraph of Section 3.3 and Fig. 3.3 of the thesis). We demonstrate this in Figure 2.3, which shows the time evolution of the effective stress in E-models within a 3 Gyr long time window taken 12 Gyr after the initiation of the simulation.

Further evolution of the models is characterized by similar stress profiles as depicted in Fig. 2.3 – the stress reduction is a general characteristic of statistically steady state viscoelastic convection with a free surface (i.e. regardless of the value of d_{TB}), as long as the lithosphere is bending and unbending in the reached statistically steady state.

For the M-models the statistically steady states are almost stationary, with a stable plume in the centre and downwellings at the sides. Due to this steady loading the lithosphere is permanently bent, and not flexing up and down as in the previous case. It then reaches the viscous limit and the effects of viscoelasticity disappear (cf. the last snapshot in Fig. 2.1).

Table 2.2 summarizes how the viscoelastic effects depend on the initial and

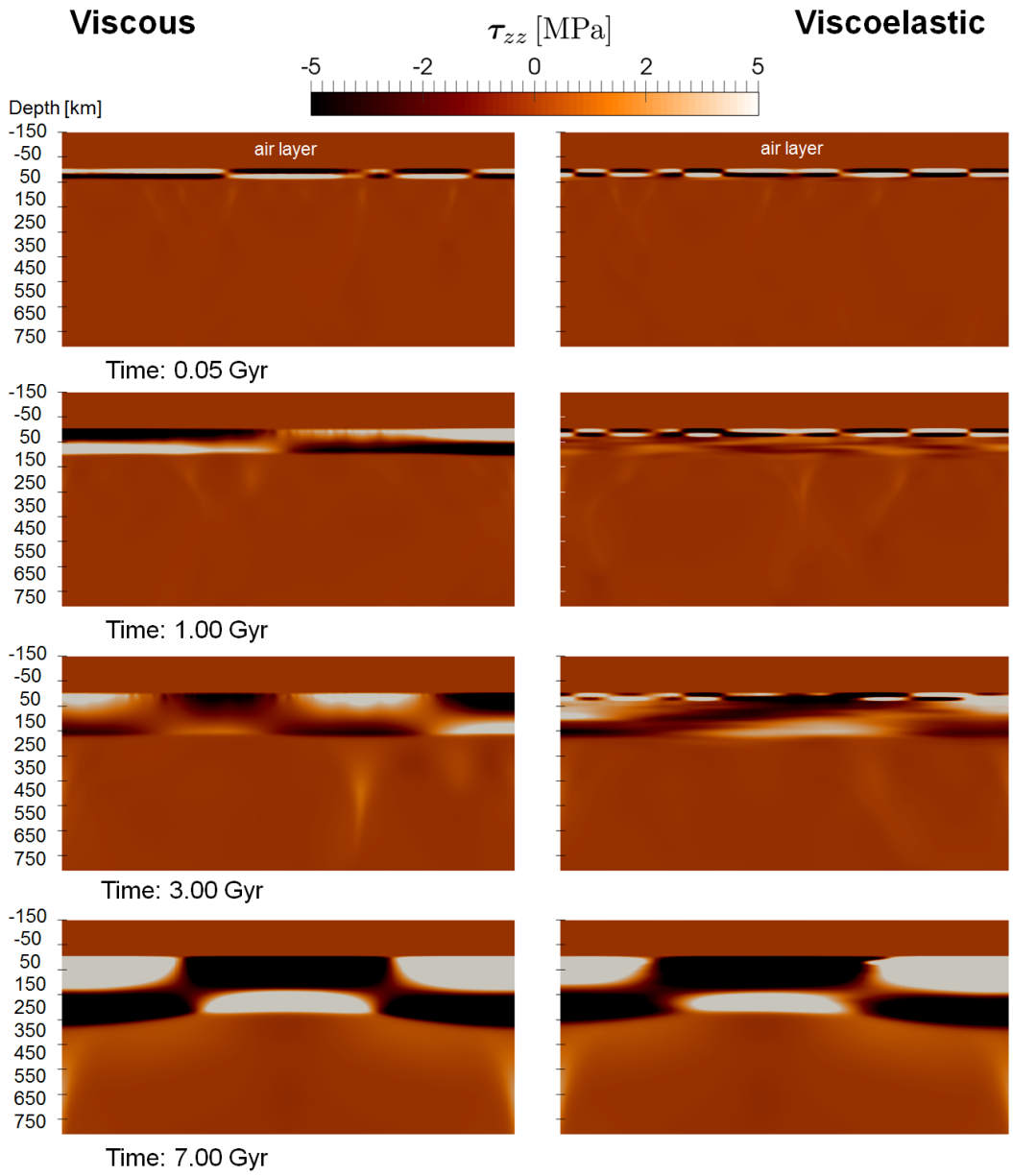

Figure 2.1: Vertical component of deviatoric stress τ_{zz} in model M with aspect ratio 1, $T_0 = 1900$ K, $d_{\mathrm{TB}} = 30$ km and a free surface. Stress scale is clipped for better visibility of the memory effect. Negative depths (in km) show the sticky air layer.

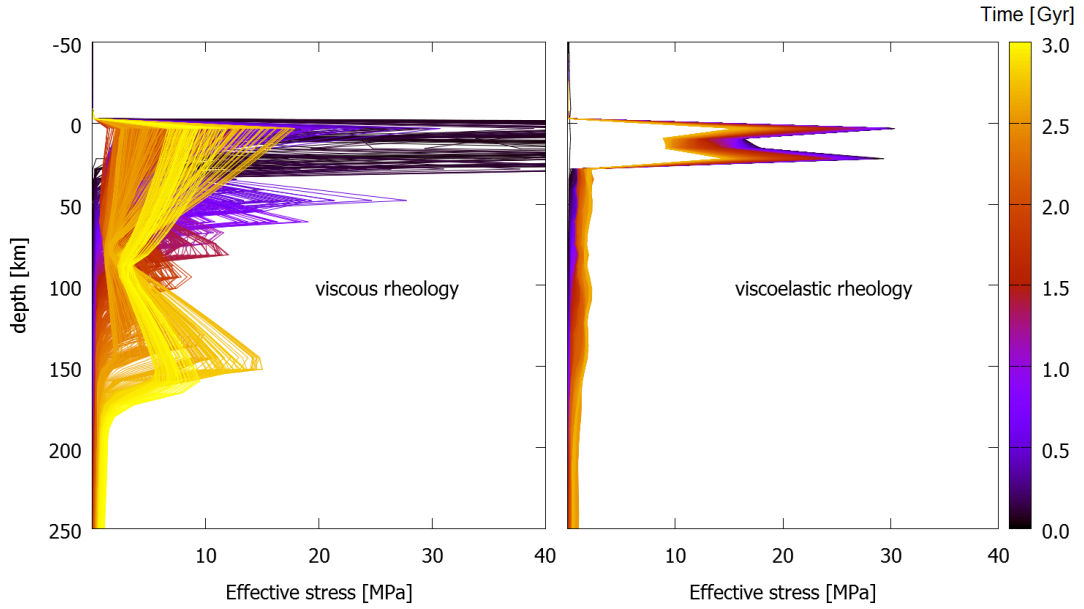

Figure 2.2: Temporal evolution of effective stress τ_{eff} in models M_{vis} and M_{el} with the same parameters as in Figure 2.1. We show horizontally averaged radial profiles that are evenly sampled in time. Colour represents the time in Gyr, only the transient behaviour is shown.

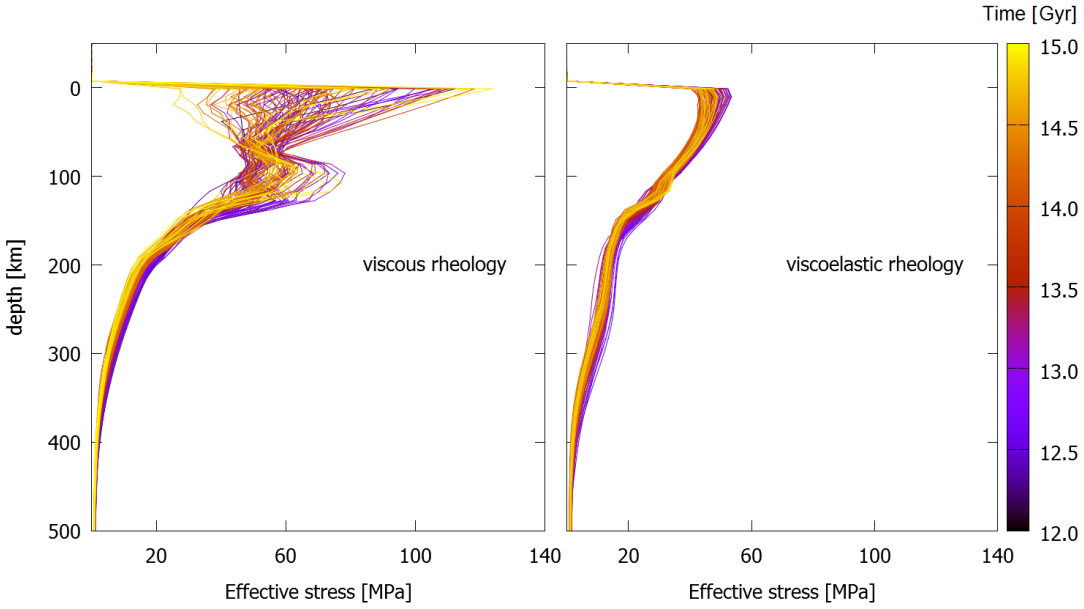

Figure 2.3: Temporal scatter of effective stress τ_{eff} in models E_{vis} and E_{el} with aspect ratio 1, $T_0 = 1900$ K, $d_{\text{TB}} = 300$ km and a free surface. We show 100 horizontally averaged depth profiles that are evenly sampled in time. Colour represents the time in Gyr.

Table 2.2: Summary of the viscoelastic effects in stagnant lid convection

Model characteristics	"Frozen-in" stresses	Stress reduction
Free-slip, initially thick lithosphere	No	No
Free-slip, initially thin lithosphere	Yes	No
Free surface, initially thick lithosphere	No	Yes
Free surface, initially thin lithosphere	Yes	Yes

boundary conditions. Both effects are stronger when the vigour of convection is higher.

Conclusions and perspectives

Numerical models that evaluate the internal deformation of planetary mantles are important for various applications. Perhaps the most unknown parameter entering such calculations is the rock rheology, with the two end-member material models being the elastic solid and viscous fluid. In the traditional view, elastic models describe the short-term behaviour and viscous models the long-term behaviour of rocks. However, there are observations implying that elasticity plays an important role in the lithosphere even on very long time scales (for a review, see Watts et al., 2013).

The medium that combines both models in a simple way – by assuming that both mechanisms are connected in series – is referred to as Maxwell-type viscoelastic material. The general idea on which the rheology is based was proposed in the 19th century, but the exact form of its constitutive equation is still subject to an open debate (see e.g. Málek & Průša, 2016). The traditional formula that appears in the literature has only the partial time derivative standing for the stress rate. However, such formula is applicable only to problems dealing with small deformations of a body. For a general deformation it is physically inconsistent because it violates the condition of material objectivity. Several objective tensor rates have been proposed to complete the traditional formula, but one is usually left without any physical argument that could help to choose a particular one, leaving the choice to experimental means. In Chapter 1 we review the physical interpretation of the commonly assumed objective tensor rates. Based on geometrical considerations, we argue that the so-called lower convected tensor rate fits the original idea of Maxwell material the best.

In studies of glacial isostatic adjustment the use of viscoelastic models has always prevailed. Postglacial rebound of the Earth's surface is essentially caused by a viscoelastic relaxation of its interior, and Maxwell model seems to provide a good first-order fit to the observed data (e.g. Sabadini et al., 2016). In Chapter 2 we investigate GIA from a rather overlooked perspective – its energetical balance. We derive a numerical tool for analyzing the changes in the rotational, gravitational, and elastic energies of a rotating planet that is subject to surface loads. The tool is used to test the accuracy of the linearized Liouville equation in determining the changes in Earth's rotation induced by GIA. We show that the predicted changes in the magnitude of the angular velocity vector are significantly affected by the linearization of the Liouville equation.

Earth's deformation associated with postglacial rebound is very small and there is no need for other than the traditional Maxwell constitutive formula. In mantle convection this is no longer the case. Chapters 3 and 4 are devoted to numerical modelling of mantle convection and assume the mantle rocks to behave as Maxwell viscoelastic fluid with the constitutive relation containing an objective stress rate. This is a step towards more realistic mantle convection models, as

present-day simulations usually ignore elasticity.

One of the primary constraints on the internal structure and dynamics of terrestrial planets is given by their surface topography. At the same time, surface topography is an observable that is likely to be affected by considering elasticity in the lithosphere, and so a number of studies have already addressed its potential effects. In Chapter 3 we compute lithospheric flexure above a rising plume in a fully viscoelastic model with a free surface and observe an elastic filtering of the resulting topography, consistently with previous findings by authors who used more simplified approaches (e.g. Golle et al., 2012).

We also observed an unforeseen effect in our mantle convection simulations. While in GIA modelling it is obvious that current deformation depends on the past (the observed uplift is caused by glaciers that no longer exist), in mantle convection this is usually not assumed. Two common exceptions, in which the internal dynamics at a given moment depend on the history of preceding flow, are simulations with grain size evolution and simulations with a predefined weak zones. In the first case, shearing can reduce the grain size in some regions, forming zones of low viscosity that further localize deformation (e.g. Rozel et al., 2011). In the latter case, predefined weak zones are supposed to represent some structural inheritance, that is, material that got weakened by deformation that preceded the numerical experiment (recently e.g. Duretz et al., 2016). We observe a new type of history dependence. When a planet cools down from its initially hot state, its lithosphere is thin at the beginning and gradually grows in thickness. Due to convective forcing, the thin lithosphere undergoes severe bending resulting in large stresses. In Chapter 3 we describe how these bending patterns can "freeze" into the growing lithosphere and are remembered there long after the sinking and rising plumes that caused the bending have disappeared. The relaxation of these features is governed by the Maxwell relaxation time of the lithosphere, which depends on the poorly constrained value of lithospheric viscosity, and can be comparable with the geological time scales.

We merely provide a proof of concept for the stress memory effect. 3-D spherical simulations that would confirm our hypothesis in a model with realistic parameters suited for a particular planet or moon are yet to be done. Especially interesting may be to study how the different spatial wavelengths of surface topography evolve throughout viscoelastic convection of a cooling planet. An ideal stagnant lid candidate seems to be the planet Mars, where the effective elastic thickness T_e of the lithosphere is observed to decrease with increasing age of surface loads (e.g. McGovern et al., 2002). This may either indicate "frozen-in" topography, consistent with the memory effect described here, or it can simply be the result of viscoelastic relaxation under the surface loads (i.e. not related to the changes of lithospheric thickness). Another open question is how much of the stress that accumulates in the initially thin lid in our simulations would get released if a realistic description of brittle and ductile yielding was involved. To answer the question, global-scale numerical simulations with complex lithospheric

rheology and high near-surface resolution must be performed.

While the behaviour of the lithosphere is altered substantially by including elasticity into mantle convection simulations, sub-lithospheric dynamics seem to be unaffected. The ability of our models to quickly build surface topography, the resistance of this process being governed by the elastic shear modulus (and not by the high value of lithospheric viscosity as in purely viscous runs), could potentially stabilize or destabilize mantle upwellings and downwellings in their spatial position, or change the number and stability of convection cells. However, we have not observed any such changes in the internal dynamics, at least for convection experiments in stagnant lid regime.

A convective regime that exhibits stronger interaction of the deep mantle with the lithosphere is the one observed on Earth. In a plate-like regime the thermal boundary layer breaks into plates which are being continuously created and subducted. One of the outstanding problems of numerical simulations of plate tectonics is that the highest possible (critical) value of yield stress that one may prescribe and still obtain a plate-like regime is much lower than the values suggested by laboratory measurements. This problem could be even worse when elastic properties of rocks are accounted for. Considering an additional deformation mechanism lowers the lithospheric resistance, reducing the convective stresses that develop in the lithosphere (to some extent, though in different settings, the effect is observed in the works of Kaus & Becker, 2007; Beuchert & Podladchikov, 2010; Thielmann et al., 2015; Patočka et al., 2017). In Chapter 4 the critical yield stress value is analyzed in a parametric study. We compare sets of visco-plastic and visco-elasto-plastic simulations with a free surface and with a free-slip surface. We find that the importance of elasticity and a free surface depends on the viscosity profile. If low viscosity is assumed, or if the viscosity exponentially decreases right below the surface (i.e. without forming an effectively elastic layer of non-negligible thickness), then little to no shift of the critical yield stress is observed. A shift appears when a high-viscosity layer several tens of km thick is assumed – the critical yield stress is higher in cases with a free surface when compared to the cases with free-slip surface. However, no first-order differences are observed between the visco-plastic and visco-elasto-plastic simulations with a free surface. This may seem surprising, because in models with comparable internal dynamics, presented in Chapter 3, the horizontally averaged lithospheric stresses differed by up to tens of MPa between viscous and viscoelastic models.

To fully understand the role of elasticity in numerical models of planetary evolution, it is necessary to perform global-scale experiments that employ complex treatment of brittle and ductile yielding in the lithosphere. The pseudoplastic yielding, commonly used to generate plate-like behaviour in global-scale convection models (e.g. Tackley, 2000), which is also used here in Chapter 4, is not suitable to capture the complexities of lithospheric deformation. Especially when low values of surface yield stress and low friction angles are employed the resulting yielding is distributed into relatively large volumes of the lithosphere instead of

forming narrow shear zones. Such behaviour disfavors the display of viscoelastic effects. These can fully develop only in settings in which elastic stresses build up in a large portion of the model domain and are subsequently released within a localized shear zone – significantly promoting the extent of deformation accommodated therein. An example of such setting was demonstrated by Jaquet et al. (2016), who performed simulations of continental collision.

The methodological division between regional and global geodynamical modelling is slowly falling apart. In numerical studies of single regions the boundary conditions are often critically questioned. It is becoming increasingly obvious that for many segments of Earth we cannot cut out a part of the mantle and model its deformation without considering the feedback from the rest of the mantle. That is, without considering how the region's boundary conditions change in reaction to what is happening inside the region. On the other hand, in global simulations of plate-like or episodic lid convection it is the lid behaviour that has first-order influence on the internal dynamics. However, regional modelling implies that a high-resolution lithosphere with non-linear, composition dependent rheology that combines various creep mechanisms is necessary to capture the lid behaviour correctly. One can thus expect the future models to be global-scale, but with complexities typical for regional-scale models. The enhancement of StagYY presented in this thesis is one of the necessary steps towards such models.

Bibliography

Armann, M. & Tackley, P. J., 2012. Simulating the thermochemical magmatic and tectonic evolution of Venus's mantle and lithosphere: Two-dimensional models, *J. Geophys. Res.*, **117**.

Beuchert, M. J. & Podladchikov, Y. Y., 2010. Viscoelastic mantle convection and lithospheric stresses, *Geophys. J. Int.*, **183**(1), 35–63.

Crameri, F. & Tackley, P. J., 2014. Spontaneous development of arcuate single-sided subduction in global 3-D mantle convection models with a free surface, *J. Geophys. Res.*, **119**(7), 5921–5942.

Duretz, T., May, D. A., Gerya, T. V., & Tackley, P. J., 2011. Discretization errors and free surface stabilization in the finite difference and marker-in-cell method for applied geodynamics: A numerical study, *Geochem. Geophys. Geosyst.*, **12**.

Duretz, T., Petri, B., Mohn, G., Schmalholz, S. M., Schenker, F. L., & Muntener, O., 2016. The importance of structural softening for the evolution and architecture of passive margins, *Scientific Reports*, **6**.

Golle, O., Dumoulin, C., Choblet, G., & Cadek, O., 2012. Topography and geoid induced by a convecting mantle beneath an elastic lithosphere, *Geophys. J. Int.*, **189**(1), 55–72.

Jaquet, Y., Duretz, T., & Schmalholz, S. M., 2016. Dramatic effect of elasticity on thermal softening and strain localization during lithospheric shortening, *Geophys. J. Int.*, **204**(2), 780–784.

Kaus, B. J. P. & Becker, T. W., 2007. Effects of elasticity on the Rayleigh-Taylor instability: implications for large-scale geodynamics, *Geophys. J. Int.*, **168**(2), 843–862.

Kaus, B. J. P., Muehlhaus, H., & May, D. A., 2010. A stabilization algorithm for geodynamic numerical simulations with a free surface, *Phys. Earth Planet. Inter.*, **181**(1-2), 12–20.

Liu, I.-S. & Sampaio, R., 2014. Remarks on material frame-indifference controversy, *Acta Mechanica*, **225**(2), 331–348.

Málek, J. & Průša, V., 2016. *Derivation of Equations for Continuum Mechanics and Thermodynamics of Fluids*, pp. 1–70, Springer International Publishing, Cham.

Málek, J. & Rajagopal, K., 2005. Chapter 5 - mathematical issues concerning the navier-stokes equations and some of its generalizations, in *Handbook of Differential Equations Evolutionary Equations*, vol. 2, pp. 371 – 459, eds Dafermos, C. & Feireisl, E., North-Holland.

Maxwell, J., 1871. Theory of heat, *Longmans, Green, and Co.*.

McGovern, P., Solomon, S., Smith, D., Zuber, M., Simons, M., Wieczorek, M., Phillips, R., Neumann, G., Aharonson, O., & Head, J., 2002. Localized gravity/topography admittance and correlation spectra on Mars: Implications for regional and global evolution, *J. Geophys. Res.*, **107**(E12).

Moresi, L., Dufour, F., & Muhlhaus, H., 2002. Mantle convection modeling with viscoelastic/brittle lithosphere: Numerical methodology and plate tectonic modeling, *Pure Appl. Geophys.*, **159**(10), 2335–2356.

Muhlhaus, H. & Regenauer-Lieb, K., 2005. Towards a self-consistent plate mantle model that includes elasticity: simple benchmarks and application to basic modes of convection, *Geophys. J. Int.*, **163**(2), 788–800.

Munk, W. H. & MacDonald, G. J. F., 1960. *Rotation of the Earth*, Cambridge University Press.

Oldroyd, J., 1950. On the formulation of rheological equations of state, *Proc. R. Soc. A*, **200**(1063), 523–541.

Patočka, V., Čadek, O., Tackley, P. J., & Čížková, H., 2017. Stress memory effect in viscoelastic stagnant lid convection, *Geophys. J. Int.*, **209**(3), 1462–1475.

Peltier, W., 2004. Global glacial isostasy and the surface of the ice-age earth: The ice-5G (VM2) model and grace, *Ann. Rev. Earth Planet Sci.*, **32**, 111–149.

Ranalli, G., 1995. *Rheology of the Earth*, Springer Netherlands.

Ricard, Y., Spada, G., & Sabadini, R., 1993. Polar wandering of a dynamic earth, *Geophys. J. Int.*, **113**(2), 284–298.

Rozel, A., 2012. Impact of grain size on the convection of terrestrial planets, *Geochem. Geophys. Geosys.*, **13**.

Rozel, A., Ricard, Y., & Bercovici, D., 2011. A thermodynamically self-consistent damage equation for grain size evolution during dynamic recrystallization, *Geophys. J. Int.*, **184**(2), 719–728.

Sabadini, R., Vermeersen, B., & Cambiotti, G., 2016. *Global Dynamics of the Earth: Applications of Viscoelastic Relaxation Theory to Solid-Earth and Planetary Geophysics*, Modern Approaches in Geophysics, Springer Netherlands.

Schaeffer, A. J., Lebedev, S., & Becker, T. W., 2016. Azimuthal seismic anisotropy in the Earth's upper mantle and the thickness of tectonic plates, *Geophys. J. Int.*, **207**(2), 901–933.

Shapiro, N. & Ritzwoller, M., 2002. Monte-Carlo inversion for a global shear-velocity model of the crust and upper mantle, *Geophys. J. Int.*, **151**(1), 88–105.

Solomatov, V., 1995. Scaling of temperature-dependent and stress-dependent viscosity convection, *Phys. Fluids*, **7**(2), 266–274.

Souček, O., Hron, J., Běhounková, M., & Čadek, O., 2016. Effect of the tiger stripes on the deformation of Saturn's moon Enceladus, *Geophys. Res. Let.*, **43**(14), 7417–7423.

Spada, G., Barletta, V. R., Klemann, V., Riva, R. E. M., Martinec, Z., Gasperini, P., Lund, B., Wolf, D., Vermeersen, L. L. A., & King, M. A., 2011. A benchmark study for glacial isostatic adjustment codes, *Geophys. J. Int.*, **185**(1), 106–132.

Tackley, P., 2000. Mantle convection and plate tectonics: Toward an integrated physical and chemical theory, *Science*, **288**(5473), 2002–2007.

Tagawa, M., Nakakuki, T., & Tajima, F., 2007. Dynamical modeling of trench retreat driven by the slab interaction with the mantle transition zone, *Earth Planets Space*, **59**(2), 65–74.

Thielmann, M., Kaus, B. J. P., & Popov, A. A., 2015. Lithospheric stresses in Rayleigh-Benard convection: effects of a free surface and a viscoelastic Maxwell rheology, *Geophys. J. Int.*, **203**(3), 2200–2219.

Tobie, G., Cadek, O., & Sotin, C., 2008. Solid tidal friction above a liquid water reservoir as the origin of the south pole hotspot on Enceladus, *Icarus*, **196**(2), 642–652.

Turcotte, D. & Schubert, G., 2002. *Geodynamics*, Cambridge University Press.

Čížková, H., van Hunen, J., & van den Berg, A., 2007. Stress distribution within subducting slabs and their deformation in the transition zone, *Phys. Earth Planet. Inter.*, **161**(3-4), 202–214.

Watts, A. B., Zhong, S. J., & Hunter, J., 2013. The Behavior of the Lithosphere on Seismic to Geologic Timescales, in *Annual Review of Earth and Planetary Sciences, Vol 41*, vol. 41, pp. 443+, ed. Jeanloz, R.

List of author's peer-reviewed publications

Patočka, V., Čadek, O., Tackley, P. J., & Čížková, H., 2017. Stress memory effect in viscoelastic stagnant lid convection, *Geophys. J. Int.*, **209**(3), 1462–1475, doi: 10.1093/gji/ggx102

Patočka, V., Čadek, O., Martinec, Z., 2018. Energy balance of glacial isostatic adjustment: importance of the rotational feedback, *Geophys. J. Int.*, **212**(2), 955–975, doi: 10.1093/gji/ggx469

Submitted

Patočka, V., Čížková, H., & Tackley, P. J., 2018. Do elasticity and a free surface affect lithospheric stresses caused by upper mantle convection?, submitted to *Geophys. J. Int.*